Polymer Chemistry

PAPER

View Article Online
View Journal | View Issue

Cite this: *Polym. Chem.*, 2019, **10**, 3127

Self-assembly of oppositely charged polyelectrolyte block copolymers containing short thermoresponsive blocks†

I. A. van Hees, [a] P. J. M. Swinkels, [b] R. G. Fokkink, [a] A. H. Velders, [c] I. K. Voets, [d] J. van der Gucht [a] and M. Kamperman *[e]

The assembly of oppositely charged block copolymers, containing small thermoresponsive moieties, was investigated as a function of salt concentration and temperature. Aqueous solutions of poly-[*N*-isopropylacrylamide]-*b*-poly[dimethylaminoethyl methacrylate] ($NIPAM_{44}$-*b*-$DMAEMA_{216}$) and PNIPAM-*b*-poly[acrylic acid]-*b*-PNIPAM ($NIPAM_{35}$-*b*-AA_{200}-*b*-$NIPAM_{35}$) were mixed in equal charge stoichiometry, and analysed by light scattering (LS), NMR spectroscopy and small angle X-ray scattering (SAXS). At room temperature, two different micelle morphologies were found at different salt concentrations. At NaCl concentrations below 0.75 M, complex coacervate core micelles (C3M) with a PNIPAM corona were formed as a result of interpolyelectrolyte complexation. At NaCl concentrations exceeding 0.75 M, the C3M micelles inverted into PNIPAM cored micelles (PCM), containing a water soluble polyelectrolyte corona. This behavior is ascribed to the salt concentration dependence of both the lower critical solution temperature (LCST) of PNIPAM, and the complex coacervation. Above 0.75 M NaCl, the PNIPAM blocks are insoluble in water at room temperature, while complexation between the polyelectrolytes is prevented because of charge screening by the salt. Upon increasing the temperature, both types of micelles display a cloud point temperature (T_{cp}), despite the small thermoresponsive blocks, and aggregate into hydrogels. These hydrogels consist of a complexed polyelectrolyte matrix with microphase separated PNIPAM domains. Controlling the morphology and aggregation of temperature sensitive polyelectrolytes can be an important tool for drug delivery systems, or the application and hardening of underwater glues.

Received 15th February 2019,
Accepted 27th March 2019

DOI: 10.1039/c9py00250b

rsc.li/polymers

Introduction

Complex coacervation is a liquid–liquid phase separation that occurs when two oppositely charged polyelectrolyte solutions are mixed, resulting in two coexisting phases: (1) the complex coacervate, a water-insoluble polyelectrolyte phase, and (2) a dilute solvent phase.[1] Complex coacervates display unique characteristics, such as a low interfacial tension and a high water content, while being water-insoluble.[2,3] This combination of properties makes complex coacervates interesting for many applications, such as underwater adhesives or encapsulants.[4–8]

The properties of complex coacervates depend on several parameters, including the chemical nature of polyelectrolytes, salt concentration, and in the case of weak polyelectrolytes, the pH. These parameters influence not only the water content, but also the interaction strength and mobility of the polyelectrolytes in the complex.[3,9] Complex coacervate core micelles (C3M) (also known as poly-ion complex (PIC) micelles, block ionomer complex (BIC) micelles, or interpolyelectrolyte complex (IPEC) micelles) can be formed when water-soluble blocks are connected to the polyelectrolytes. These water-soluble blocks will form a stabilizing corona around the water-insoluble complex coacervate core of the C3M.[9–11]

A special class of C3Ms are stimuli responsive micelles, which are promising systems for sensors or controlled delivery systems, and many reports describe C3Ms that are responsive to ionic strength, pH or temperature.[9,12–20] Most of these C3Ms are designed to be stable in solution, which is important

[a]*Physical Chemistry and Soft Matter, Wageningen University and Research, Stippeneng 4, 6708 WE Wageningen, The Netherlands*
[b]*Institute of Physics, University of Amsterdam, Science Park 904, 1098 XH Amsterdam, the Netherlands*
[c]*Laboratory of BioNanoTechnology, Wageningen University and Research, Bornse Weilanden 9, 6708 WG Wageningen, The Netherlands*
[d]*Department of Chemical Engineering and Chemistry, Eindhoven University of Technology, P.O. Box 513, 5600 MB Eindhoven, The Netherlands*
[e]*Polymer Science, Zernike Institute for Advanced Materials, University of Groningen, Nijenborgh 4, 9747 AG Groningen, The Netherlands.*
E-mail: marleen.kamperman@rug.nl

†Electronic supplementary information (ESI) available. See DOI: 10.1039/c9py00250b

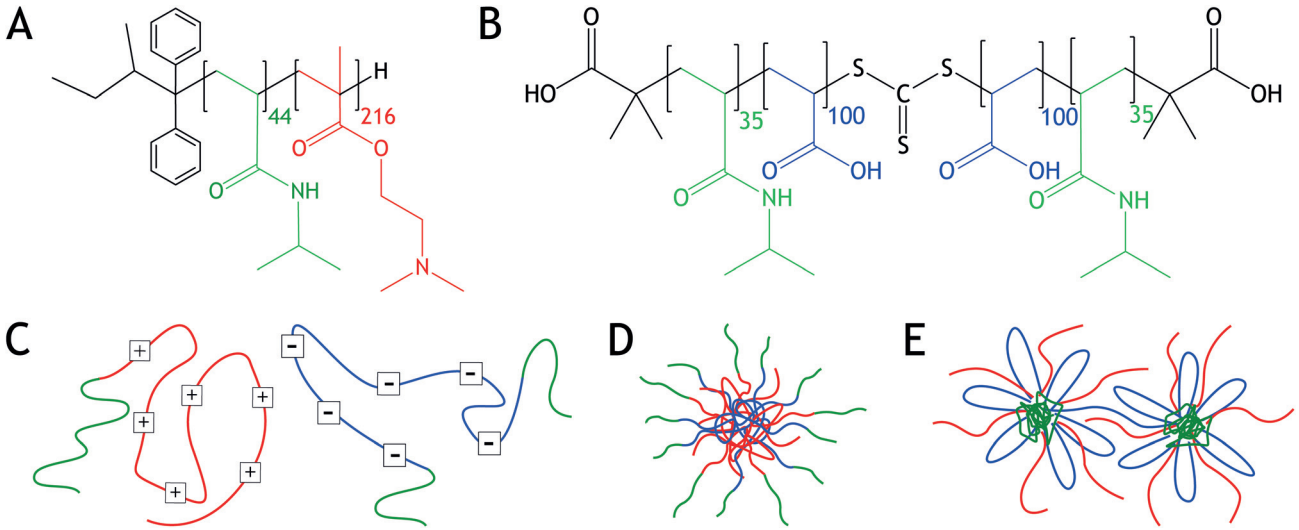

Fig. 1 Chemical structures of (a) cationic PNIPAM-*b*-PDMAEMA, which was synthesized by anionic polymerization, and (b) PNIPAM-*b*-PAA-*b*-PNIPAM, which was synthesized by reversible addition fragmentation chain transfer (RAFT) polymerization. Schematic representations of (c) PNIPAM-*b*-PDMAEMA and PNIPAM-*b*-PAA-*b*-PNIPAM, (d) a C3M, and (e) PCMs. The red block represents PDMAEMA, the blue block PAA and the green blocks PNIPAM.

for applications such as drug delivery. Therefore, large stabilizing blocks with a minimum block length of 30 mol% are typically used to form the corona.[13–18] However, for applications such as adhesives, the formation of a dense solid phase is needed and smaller temperature responsive blocks may be preferred to obtain a different morphology.

In this article, we study the assembly of oppositely charged block copolymers with short temperature-sensitive blocks. The system is composed of two *block*-copolymers, poly-[*N*-isopropylacrylamide]-*b*-poly[dimethylaminoethyl methacrylate] (PNIPAM-*b*-PDMAEMA) and PNIPAM-*b*-poly[acrylic acid]-*b*-PNIPAM (PNIPAM-*b*-PAA-*b*-PNIPAM) (Fig. 1). Both PDMAEMA and PAA are weak polyelectrolytes that are positively and negatively charged at neutral pH, respectively, therewith enabling complex coacervation.[1,3] Thermo-responsiveness is introduced into the system by means of PNIPAM, which is a well-explored polymer displaying a lower critical solution temperature (LCST).[21] Below the LCST, PNIPAM is water-soluble, while above the LCST, the polymer chain collapses and PNIPAM becomes water-insoluble.[22] The LCST of PNIPAM in aqueous solution is about 32 °C, but varies with molecular weight, salt concentration, and block length ratio when copolymerized.[22–25]

We study both the influence of salt concentration and temperature on the morphology of the block copolymer mixtures. Analysis is performed using light scattering (LS), nuclear magnetic resonance spectroscopy (NMR), and small angle X-ray scattering (SAXS). We show that at low salt concentrations, C3Ms with a PNIPAM corona are formed, Fig. 1. However, sufficiently elevated salt concentrations turn the C3Ms inside out, leading to PNIPAM-cored micelles (PCMs) with a water-soluble polyelectrolyte corona. Upon temperature increase, both C3Ms and PCMs aggregate and form hydrogels, displaying a salt concentration dependent cloud point temperature (T_{cp}).

Experimental

Materials

1,4-Dioxane (99.8%), NIPAM (97%), azobisisobutyronitrile (AIBN) (98%), *tert*-butyl acrylate (98%, 10–20 ppm monomethyl ether hydroquinone inhibitor), aluminium oxide (neutral, Brockmann I) and hydrochloric acid (37%, RG) were purchased from Sigma Aldrich and used as received, unless mentioned otherwise. Sodium chloride (>99.5%) was bought from Acros Organics. Methanol (HPLC grade), dichloromethane (DCM) (AR), diethyl ether (AR), 1,1,1,3,3,3-hexafluoro-2-propanol (HFIP) (AR) and *n*-hexane (HPLC grade) were purchased from Biosolve and used as received, unless mentioned otherwise. Sodium hydroxide solution (TitriPUR, 0.1 M) was bought from Merck Chemicals. PNIPAM-*b*-PDMAEMA was purchased from Polymer Source, M_n 38.2 kDa and PDI 1.05, ESI Fig. 1.† The chain transfer agent *S*,*S*′-bis(α,α′-dimethyl-α″-acetic acid) trithiocarbonate (BDAT) was synthesized using a previously described method.[26,27]

Triblock synthesis and characterization

Synthesis of poly-(*N*-isopropylacrylamide). NIPAM was recrystallized twice from *n*-hexane. AIBN was recrystallized from methanol prior to use. A round bottom flask was filled with 30.9 mg AIBN, 266 mg BDAT, 8.5 g NIPAM, and 43 mL dioxane (m : R : i as 80 : 1 : 0.2, [m] 0.8 M). The reactants were dissolved and the mixture was purged with nitrogen for 60 minutes. The polymerization took place at 70 °C for 85 minutes. Subsequently, the reaction was quenched by

exposure to air and rapid cooling. The resulting polymer was purified by precipitation in diethyl ether. The final product was dried under vacuum. ^{1}H-NMR (400 MHz, D_2O, ESI Fig. 2†): δ 1.05 (s, 6H), 1.36–2.1 (m, 3H), 3.80 (s, 1H), 6.24 (s, 1H). GPC: M_n 7.6 kDa and PDI 1.26.

Synthesis of poly[[*N*-isopropylacrylamide]-*b*-acrylic acid-*b*-[*N*-isopropylacrylamide]]. *tert*-Butyl acrylate was run over an alumina column to remove the inhibitor. AIBN was recrystallized from methanol. A round bottom flask was loaded with 16.4 mg AIBN, 4.1 g poly-NIPAM macro-CTA, 24.4 g *tert*-butyl acrylate and 48 mL dioxane (m : R : i as 380 : 1 : 0.2, [m] 3.9 M). The reactants were dissolved and the mixture was purged with nitrogen for 60 minutes. The polymerization took place for 55 minutes at 70 °C. The reaction was quenched by exposure to air and rapid cooling. The polymer was purified by precipitation in a cold methanol/water mixture, 3/1 v/v. A dry product was obtained by redissolving in minimal DCM and subsequent drying under vacuum. ^{1}H-NMR (400 MHz, $CDCl_3$): δ 1.11 (s, 6H, $(CH_2)_2$ isopropyl), 1.4–1.5 (s, 9H, $(CH_3)_3$ *tert*-butyl), 1.6–2.2 (m, backbone), 3.99 (s, 1H, CH isopropyl). ^{13}C-NMR (400 MHz, MeOD): δ 22.38 ($(CH_3)_2$ isopropyl), 28.07 ($(CH_3)_3$ *tert*-butyl), 36–40 (backbone), 41.9 (CH isopropyl), 42.38 (backbone), 174.12 ((C═O)N acrylamide).

The resulting *tert*-butyl acrylate copolymer was deprotected by dissolving in HFIP containing 0.12 M hydrochloric acid and the mixture was stirred for 3 hours.[28] The sample was dried under vacuum and redissolved in water, by adding a 0.1 M sodium hydroxide solution. The polymer solution was centrifuged to remove any insoluble by-products of the deprotection and was further purified by dialysis. The final product was obtained after freeze drying. ^{1}H-NMR (400 MHz, MeOD, ESI Fig. 3†): δ 1.16 (s, 6H, $(CH_3)_2$ isopropyl), 1.4–2.3 (m, backbone), 3.97 (s, 1H, CH isopropyl). ^{13}C-NMR (400 MHz, D_2O, ESI Fig. 4†): δ 21.65 ($(CH_3)_2$ isopropyl), 35–40 (backbone), 41.8 (CH isopropyl), 44.80 (backbone), 175.4 ((C═O)N acrylamide), 183.4 ((C═O)OH carboxylic acid). GPC: M_n 26.8 kDa and PDI 1.59.

Polymer characterization. NMR was used to determine the purity of all the products and the conversion of the monomers in polymerization. ^{1}H and ^{13}C NMR-spectroscopy measurements were carried out on a Bruker AMX-400 spectrometer (400 MHz) at room temperature. Gel permeation chromatography (GPC) of the PNIPAM macroRAFT agent was performed using an Omnisec Reveal system with an Omnisec Resolve detector, equipped with two PSS PFG columns. The samples were run in 1,1,1,3,3,3-hexafluor-2-isopropanol containing 0.02 M potassium trifluoroacetate. GPC of the triblock was carried out with an Agilent 1260 Infinity II HPLC gel permeation chromatograph, equipped with a Waters Ultrahydrogel500 column. The samples were run using an aqueous buffer of 0.01 M Na_2HPO_4/NaH_2PO_4 with 0.1 M $NaNO_3$ as an eluent.

Methods

Sample preparation. The polymers were dissolved in water as stock solutions with a concentration of max. 300 g L^{-1} and the pH was adjusted to 6.5 ± 0.2. Samples were prepared by making a NaCl solution with the desired salt concentration. First, the polyanion was added to the salt solution, followed by the polycation, such that the total final chargeable monomer concentration was 0.1 M. The order of mixing is important as it determines the degree of coacervation. Also, the polymers were added in an equal charge stoichiometry, meaning that the amount of positively charged monomers equals the amount of negatively charged monomers, as was verified by zetapotential measurements that should result in about 0 mV (ESI Fig. 7†). The solution was shaken and refrigerated to equilibrate before use.

Zetapotential measurements. Charge stoichiometry was verified using zetapotential measurements. All measurements were performed using a Malvern Zetasizer Nano ZS (Malvern Instruments, U.K.) at 25 °C after a temperature equilibration time of 30 s. The number of runs was selected automatically using the Zetasizer software (version 7.02, Malvern Instruments, U.K.). A 4 mW He–Ne ion laser at 633 nm was used and the signal was detected at a fixed angle of 173°. Each measurement was repeated six times. Samples were prepared at 0.5 M NaCl and 0.1 M charged monomers, followed by three-fold dilution using demineralised water.

Light scattering. LS experiments were performed on an ALV CGS-3 compact goniometer system equipped with a JDSU 1145P laser, operating at a wavelength of 633 nm, and an ALV/LSE-5004 external correlator. The measurements were carried out at a measuring angle of 90°. The data were analysed with a second order cumulant fit using ALV-7004 Correlator software and checked for monodispersity using CONTIN. The temperature was controlled with a Julabo Refrigerated–Heating Circulator. The temperature increased in steps of 2 °C, using a time interval of 10 minutes. This time is sufficient to equilibrate the micelles, as waiting steps of 1 hour yielded similar results. Furthermore, samples containing a charged monomer concentration of 0.1 M were used and demonstrated radii similar to samples containing 0.01 M charged monomers. Therefore, we assumed that interparticle interactions do not influence the results at the used concentration.

LS was used to determine the cloud point temperature T_{cp}. In this article, the T_{cp} of the assemblies is defined as the temperature where the scattering intensity has doubled compared to its value at 17 °C for 0.75 M NaCl, and 25 °C for all other samples. The data used for this determination are shown in ESI Fig. 8.†

NMR. 1D ^{1}H and 2D ^{1}H^{1}H-NOESY NMR experiments were performed on a Bruker AVANCE 600 NMR spectrometer equipped with a TCI cryoprobe. Standard Bruker pulse sequences were used with typical mixing times for the NOESY experiments of 100 ms. 90 degree pulses were calibrated for each sample to account for the high salt concentrations.

Small angle X-ray scattering. SAXS measurements were performed on a SAXSLAB GANESHA 300 XL SAXS machine equipped with a GeniX 3D Cu Ultra Low Divergence microfocus sealed tube source producing X-rays with a wavelength of λ = 1.54 Å at a flux of 15.8 × 10^6 ph s^{-1} and a Pilatus 300 K silicon pixel detector with 487 × 619 pixels of 172 μm^2 in size

placed at a sample-to-detector distance of 441 mm and/or 1041 mm to access a q-range of $0.004 \leq q \leq 0.710$ Å^{-1}, and a q-range of $0.003 \leq q \leq 0.296$ Å^{-1} with $q = 4\pi/\lambda(\sin\theta)$, where 2θ represents the observation angle. Silver behenate was used for the calibration of the beam centre and the q-range. Samples were contained in 2 mm quartz capillaries (Hilgenberg GmbH, Germany) and the temperature was controlled using a Julabo heating circulator. The two-dimensional SAXS patterns were azimuthally averaged to obtain one-dimensional SAXS profiles.

Results and discussion

NaCl concentrations up to 0.75 M

Light scattering. In this section, samples containing up to 0.75 M NaCl will be discussed, while samples with higher salt concentrations will be discussed below. The described block copolymers were mixed at different NaCl concentrations, at constant pH, and equal charge. The charge fraction, $f^+ = \frac{n^+}{n^+ + n^-}$, was set at 0.5 (ESI Fig. 7†) by adding equal amounts of DMAEMA and AA monomers, which should approximately result in a net zero charge at pH 6.5. To verify this, zetapotential measurements were performed, and the ratio between the monomers was adjusted when needed. The samples were investigated using light scattering while increasing the temperature (ESI Fig. 8†). At room temperature, a single phase is observed, while at elevated temperatures, an aggregated system is found. To show the transition between these systems, a summary of the LS data is given in Fig. 2. In the single phase system at salt concentrations below 0.75 M, most often objects with well-defined and monodisperse hydrodynamic radii are observed at room temperature (ESI Fig. 9†). CONTIN analysis revealed a monomodal decorrelation curve, suggesting the assembly of the polymers into well-defined objects, such as C3Ms.

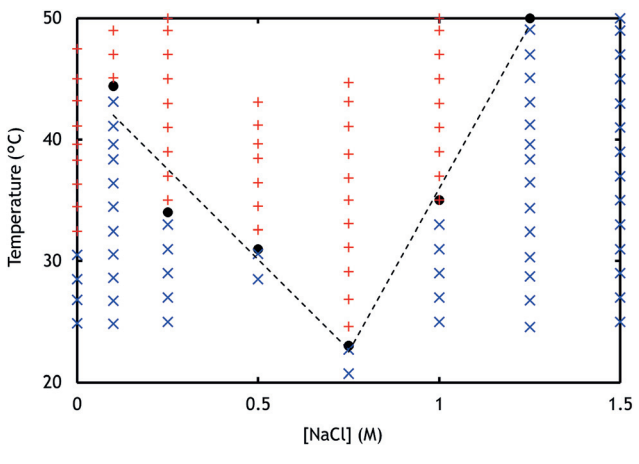

Fig. 2 Light scattering was used to determine the T_{cp} of samples containing PNIPAM-*b*-PDMAEMA and PNIPAM-*b*-PAA-*b*-PNIPAM with varying concentrations of NaCl. The results were used to create a phase diagram; the blue crosses represent a one phase system, and the red plusses represent an aggregated system. The dotted lines represent the phase boundary that was deduced from the observed T_{cp}s (black dots).

The assembly of the polymers into C3Ms can be explained by the interactions between the polyelectrolytes and the solubility of PNIPAM under these conditions. Mixed homopolymers of PDMAEMA and PAA, of block lengths comparable to the electrolyte blocks used in this research, form complexes below the critical salt concentration (c_s) of approximately 1.1 M NaCl.[3] This means that below 0.75 M NaCl, complex coacervation between the PDMAEMA and PAA blocks can occur. PNIPAM, on the other hand, is soluble at room temperature and at salt concentrations of 0.75 M NaCl and below. Regarding the well-defined objects observed in LS, the PNIPAM blocks are able to solubilize the complexed polyelectrolytes, resulting in C3Ms with a PNIPAM corona.

From LS, an estimated size for the C3Ms can be obtained. For 0.5 M NaCl, an R_h of 31 nm was observed. This value is similar to values that were reported before.[9,13] By using LS, Voets *et al.* observed C3Ms with an apparent R_h of 31.3 ± 0.9 nm that were composed of poly(*N*-methyl-2-vinyl pyridinium iodide)-*b*-poly(ethylene oxide), $PM2VP_{38}$-*b*-PEO_{211}, and PAA_{55}-*b*-$PNIPAM_{88}$. Park *et al.* observed micelles upon mixing poly(2-isopropyl-2-oxazoline)-*b*-poly(lysine), $PiPrOx_{45}$-*b*-$P(Lys)_{85}$, PiPrOx-*b*-poly(aspartic acid), and $PiPrOx_{45}$-*b*-$P(Asp)_{76}$, with an apparent R_h of 22.6 nm by LS.

Upon sufficient temperature increase, the aggregation of the micelles from solution was observed as is indicated by a sudden increase in the radius, scattering intensity, and/or polydispersity in the LS data (ESI Fig. 8 and 10†).[17] In Fig. 2, the determined T_{cp} (black dots) are shown for all the measured salt concentrations. It was observed that below 0.75 M NaCl, the T_{cp} decreases with increasing salt concentration. This trend can be attributed to the salt concentration dependent solubility of PNIPAM. PNIPAM solubility decreases when salt concentrations increase, which is expressed by a decreasing LCST and thus collapsing of the polymer chain at lower temperatures (ESI Fig. 21†).[23,29] A similar behaviour was observed not only for PNIPAM containing micelles but also for micelles containing different temperature-responsive blocks.[13] After sufficient cooling of the samples, aggregates disappeared again and radii similar to the sizes observed before heating were measured, demonstrating the reversibility of the system.

The T_{cp} observed at 0 M NaCl deviates from the tendency of increasing T_{cp} with decreasing salt concentration. Without added salt, oppositely charged polyelectrolytes strongly interact immediately upon mixing, through electrostatic bonds with long relaxation times. This most likely results in a heterogeneous and kinetically trapped system. The system may not have enough mobility to arrange in stable micelles, which in turn will result in a lower T_{cp}.

NMR. NMR is used to verify the presence of C3Ms at 0.5 M salt concentration. In the ^{1}H spectra of the mixtures, as shown in Fig. 3, the peaks of the backbone between 1.0 and 2.2 ppm are broadened compared to the unmixed PDMAEMA and PAA (ESI Fig. 11 and 12†). Also, the peak of PDMAEMA (peak A) at 2.9 ppm is broadened. Peak broadening occurs when the mobility, and thus solubility, of the molecules is decreased, *e.g.* in the case of complexation. In contrast, the PNIPAM peak

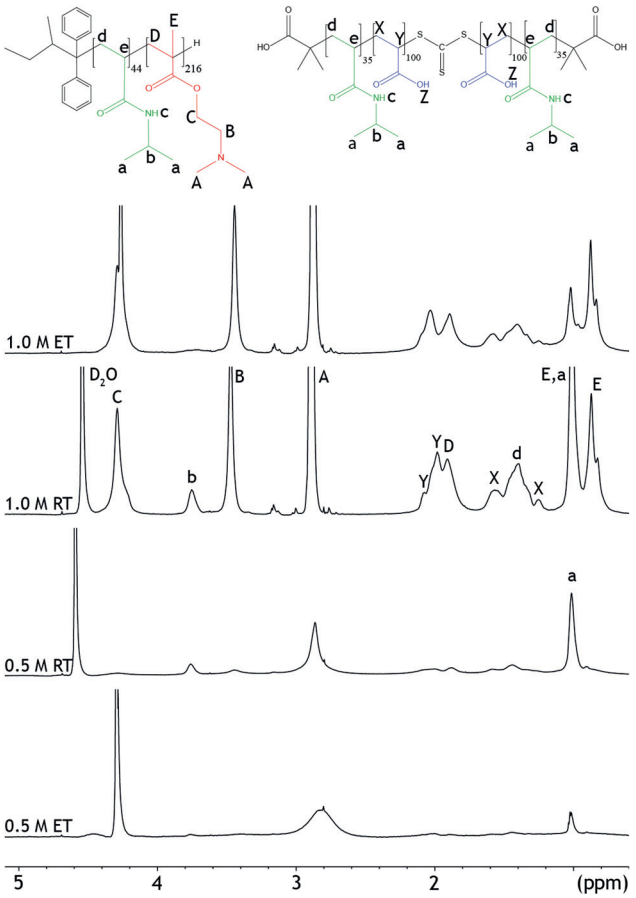

Fig. 3 ^{1}H-NMR spectra of mixtures of PNIPAM-*b*-PDMAEMA and PNIPAM-*b*-PAA-*b*-PNIPAM in 0.5 M and 1.0 NaCl, at 27 °C (RT), and 67 °C (ET).

at 3.8 ppm remained sharp, which shows an unchanged mobility of the PNIPAM blocks.

NOESY-NMR is a 2D-NMR technique that establishes correlations between chemical moieties that are in close proximity through space, *i.e.* within 1 nm distance from each other. Therefore, this NMR technique can also be used to verify the proposed micelle morphologies.[14] ESI Fig. 15† depicts the NOESY spectrum at 0.5 M NaCl. A cross-peak between the PDMAEMA and PAA (2.1;2.9) can be observed in the spectrum at room temperature.

Furthermore, cross-peaks can be observed between peaks belonging to the same polymer block, *e.g.* for PNIPAM peak b at 3.9 ppm. In NOESY spectra obtained from unmixed polymer solutions, cross-peaks can only be observed between PNIPAM peaks, or only between polyelectrolyte peaks (ESI Fig. 19 and 20†). Altogether, the data show that PAA and PDMAEMA are close in space when the polymers are mixed. Therefore, both 1D and 2D NMR techniques indicate the presence of C3Ms, with a water insoluble complex coacervate core and a hydrated PNIPAM corona at low salt concentration and temperature.

Additionally, NMR experiments were performed at elevated temperatures to investigate whether the aggregation of the micelles leads to differences in the morphology between the samples at different salt concentrations. At 67 °C, the peak splitting and peak intensities of the PDMAEMA (peaks A and B), and the PNIPAM (peaks a and b) decreased even further, Fig. 3. This reflects the decreased solubility of the micelles at elevated temperatures. In NOESY, cross-peaks that were present between DMAEMA and PAA at room temperature disappeared after increasing the temperature (ESI Fig. 16†). Both observations can be explained by the reduced solubility of the polymers resulting from the aggregation, which reduces visibility in NMR. After cooling the samples back to room temperature, similar ^{1}H spectra could be obtained as before heating, showing the reversibility of the system (ESI Fig. 13†).

Small angle X-ray scattering. SAXS measurements were performed to investigate the size and shape of the micelles at room temperature, and the morphological features of the hydrogels at elevated temperatures. The scattering intensity of the 0.5 M NaCl sample at room temperature was low, which resulted in noisy data after 8 h of data collection, see Fig. 4A. As a result, we limit ourselves to a qualitative description of the scattering curves. The slope in the q-range of 0.03 – 0.2 Å^{-1} is estimated to be −2. For spheres or micelles with a sufficient density difference between the core and the corona, a slope of −4 is expected. Therefore, we suggest that the micelle has an indistinct boundary between the core and the corona, which is the result of the high water content of the complex coacervate core. Alternatively, the limited stability of the samples (see discussion in the next session) may have resulted in aggregation, which in turn may have reduced the concentration of the micelles significantly, resulting in poor scattering.

The SAXS spectra at an elevated temperature exhibit more morphological features compared to the spectra at room temperature. At 67 °C, a peak appears at 0.032 Å^{-1}, corresponding to a characteristic distance of approximately 20 nm. It is plausible that the observed distance corresponds to the typical distance between PNIPAM and complex coacervate domains. However, the lack of higher order peaks suggests that there is no specific long range arrangement of the domains.

Sample stability. In this research, all samples were prepared at charge neutrality, as was checked by zetapotential measurements. Equal charge ratios appeared to be a requirement for obtaining macroscopic aggregation, and for the sudden steep increase in the radius, scattering intensity and polydispersity that were observed in LS. Samples prepared at non-equal charge stoichiometry displayed T_{cp} like behaviour, but showed a more gradual increase in the radius and scattering intensity. This behaviour can be explained by the presence of like-charged micelles with an excess charge in the corona, leading to repulsion between the micelles and at sufficient net charge prevention of macroscopic aggregation.[11,32] Similarly, PNIPAM that was copolymerized with hydrophilic moieties also showed a more gradual aggregation.[30]

To obtain monodisperse micelle solutions, the equilibration of the samples is a key factor. Immediately after the preparation of the 0.5 M NaCl samples, small pieces with a gel like structure appeared in the 0.5 M NaCl solutions and dissolved over time. The dissolution of these solid pieces could

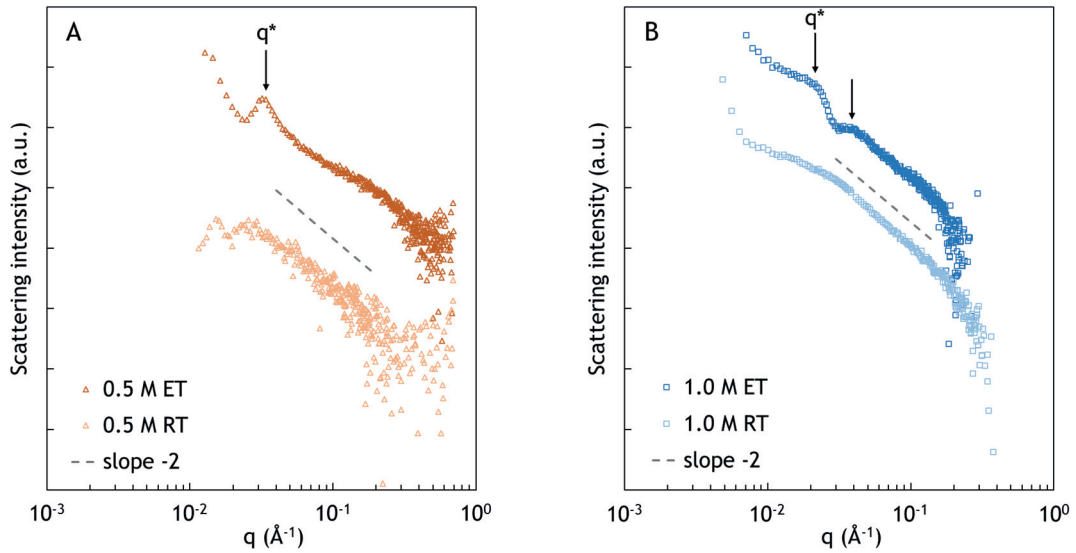

Fig. 4 SAXS spectra of PNIPAM-*b*-PDMAEMA and PNIPAM-*b*-PAA-*b*-PNIPAM in 0.5 M (A) and 1.0 M (B) NaCl at 27 °C (RT) and 67 °C (ET). As a guide to the eye, a dashed line is displayed to indicate a slope of −2. The presented data were corrected for solvent contributions and plotted on a log–log scale. Scattering intensities of the ET data were adjusted for clear display.

be sped up by refrigerating, which is also reported by Park *et al.*[13] Furthermore, for elevated polymer concentrations at room temperature, micelle solutions at low salt concentrations were not fully stable and after one day, sediments of a complex coacervate coexisted with a dilute phase which contained micelles. This observation can be explained by the short PNIPAM chains that are likely not able to completely stabilize the micelles in solutions with higher polymer concentrations, resulting in aggregation and sedimentation. A similar behaviour was observed by De Santis *et al.* who investigated C3Ms with different sizes of water-soluble blocks.[17] Micelles composed of block copolymers with the smallest stabilizing blocks formed aggregates, while the other micelles did not. Bayati *et al.* also observed the aggregation of PNIPAM-containing micelles but underlined that PNIPAM can not only aggregate above the LCST, but also below the LCST due to weak hydrophobic interactions, leading to aggregation as well.[14] Furthermore, they observed that increasing polymer concentrations resulted in increased aggregation, similar to our findings.

NaCl concentrations from 0.75 M and above

Light scattering. Preparing samples at NaCl concentrations of 0.75 M, and above, at room temperature, resulted in objects with high polydispersities, as observed from the PDI from LS (ESI Fig. 9†), and displayed multimodal decorrelations in the CONTIN analysis. The formation of objects under these conditions is unexpected as the formation of coacervates, and thus C3Ms, is prevented when the salt concentration exceeds a critical salt concentration ($c_{s,cr}$), which is at about 1.0 M NaCl for this system. Above 0.75 M NaCl, PNIPAM is insoluble at room temperature which leads to the formation of micelles consisting of an insoluble PNIPAM core, stabilized by the polyelectrolytes (PCMs) (ESI Fig. 21†).

With LS, polydisperse structures are observed. As a control, angle dependent LS was performed on samples containing 1.25 M NaCl and 0.01 M charged groups. These measurements resulted in a linear relationship between the decay rate Γ and q^2, which only slightly deviated at high q. The linear decay indicates the presence of spherical particles at elevated salt concentrations, instead of, for example, cylindrical objects. The triblock PNIPAM-*b*-PAA-*b*-PNIPAM can form bridges between the different micelles, as is schematically shown in Fig. 1e. The presence of interconnected micelles at higher polymer concentrations could be an explanation for the polydisperse structures observed with LS.

For PCMs, aggregation is observed with increasing T_{cp} for higher salt concentrations, Fig. 2, while at lower salt concentrations, a decrease in T_{cp} was observed. The aggregation of PCMs is caused by the reoccurrence of complexation of the polyelectrolytes, which can be explained by two phenomena. Firstly, complex coacervation is most likely entropically driven, thus temperature dependent.[31] Secondly, by increasing the temperature, the $c_{s,cr}$ also increases. When $c_{s,cr}$ exceeds the salt concentration of the sample, complex coacervates can be formed. For higher salt concentrations, higher temperatures are needed to exceed the $c_{s,cr}$. This behaviour was observed before for PAA/PDMAEMA homopolymers and in addition to other homopolymer couples, such as poly(trimethyl amino ethyl methacrylate) (PTMAEMA) and poly(sulphopropyl methacrylate) (PSPMA).[31] The influence of the LCST of PDMAEMA on the aggregation at a high salt concentration is considered unlikely, as charges on the polyelectrolyte prevent LCST behaviour. At this pH, the PDMAEMA is charged, and the charges cannot be screened by PAA due to the high salt concentration. Increasing T_{cp} with increasing NaCl concentrations is therefore likely the result of increased polyelectrolyte solubility, and a complex coacervation-driven aggregation of the PCMs.

With LS, different tendencies in the radii can be observed with increasing temperature, between the samples at low and high salt concentrations, ESI Fig. 8.† Below 1.0 M NaCl, the radius steeply increases with increasing temperature, while at a high salt concentration, first a decrease in the radius is observed, followed by an increase. This tendency might be explained by a collapse of either the core or the corona preceding aggregation.[32] As a result, the scattering intensity would increase while the micellar radius decreases, as is observed at 1.0 M NaCl.

Equal to samples containing less than 0.75 M NaCl, sedimentation was observed for the samples prepared above 0.75 M NaCl. However, the sedimentation only occurred after a couple of days. The polyelectrolyte blocks of the PCMs are much larger than the insoluble PNIPAM blocks under these conditions and therefore more efficiently stabilize the micelles without aggregating. Therefore, higher polymer concentrations could also be obtained without visible aggregation within a day.

NMR. For 1.0 M NaCl, similar peak patterns are observed when comparing the 1D spectra of unmixed and mixed polymers. Also, when comparing the polymer mixtures at 0.5 and 1.0 M NaCl, the peak intensity is higher and the peak splitting is more defined at increased salt concentrations, Fig. 3. This indicates a higher mobility, and thus a higher solubility of the polymers at high salt concentrations. Furthermore, in the NOESY spectra, no cross-peaks between PDMAEMA and PAA can be observed at room temperature for representative resonances at 2.1 and 2.9 ppm, ESI Fig. 17.† This can be caused by an inability of the system to detect nuclear Overhauser cross-peaks, for example due to low solubility of the polymers or due to a large distance between the polymers. From the proton spectra, it is known that the polymers have a high mobility, and therefore it is most likely that correlations are not present on the timescale of the measurement, because of a larger separation of the polyelectrolyte blocks. Together, this supports the hypothesis of the presence of PCMs with a dehydrated PNIPAM core and a hydrated polyelectrolyte corona at high salt concentrations.

At 67 °C, the intensity of the peaks has slightly decreased and the proton peak of the PNIPAM has even disappeared, Fig. 3. This indicates a reduced solubility at temperatures above the LCST. Also at this salt concentration, the temperature transition is a reversible process, ESI Fig. 14.† Furthermore, cross-peaks between PDMAEMA and PAA, 2.1;2.9 ppm, appear in the NOESY spectra when the temperature is increased, ESI Fig. 18.† The appearance of the cross-peaks indicates reoccurring complex coacervation at elevated temperatures.[33]

Small angle X-ray scattering. At 1.0 M NaCl, the scattering intensity is higher as compared to 0.5 M NaCl, because of the denser core and thus, a higher density difference between the core and the solvent, which resulted in higher scattering intensities. At room temperature, a slope of −2 can be observed from $q \approx 0.03$ until 0.2 $Å^{-1}$. As spherical particles are expected from the multi-angle LS results, we expect a similar morphology to that of 0.5 M NaCl samples, *i.e.* a weak distinction between the core and the corona, causing a lower slope. At low q values, an upturn in the scattering intensity is observed, which is ascribed to the presence of larger sized objects.[18,33] These objects may form upon bridge formation between micelles.

At elevated temperature, two broad peaks can be observed at approximately 0.021 and 0.037 $Å^{-1}$, as is indicated with the black arrows in Fig. 4B. Similar to 0.5 M NaCl, the peaks likely originate from a typical distance between PNIPAM and complex coacervate domains. The broad higher order peak at $q \approx 0.037$ $Å^{-1}$ indicates ordering over longer distances. However, the shape and order of the domains cannot be determined from the spectrum. From q^*, the characteristic distance between the domains is calculated as approximately 30 nm.[34–37] Compared to the sample at 0.5 M NaCl, the characteristic distance is larger, which could be related to the difference in the salt concentration, and thus the difference in the water content, as was also observed in the peak splitting in NOESY-NMR. The sample with a high salt concentration has weaker interpolyelectrolyte interactions, leading to a looser structure and lower polymer concentration, and thus larger distances between the PNIPAM domains, as was also found by Krogstad *et al.*[3,34]

Conclusions

By mixing oppositely charged polyelectrolytes functionalized with PNIPAM, different micelle morphologies could be obtained at room temperature. At low salt concentrations, C3Ms were observed with a PNIPAM corona and a polyelectrolyte core. At sufficiently high salt concentrations, the micelles turned inside out, into PCMs with a water-soluble polyelectrolyte corona and a PNIPAM core. Both micelles displayed a salt dependent T_{cp}, leading to aggregation and sedimentation in aqueous solution. The resulting concentrated phase contains domains of PNIPAM and complex coacervate with a salt concentration dependent separation distance. The ability to adjust the morphology and solubility of the micelles can be an important tool to apply complex coacervates as drug delivery vehicles, or as underwater or medical adhesives.

Conflicts of interest

There are no conflicts of interest to declare.

Acknowledgements

The authors thank Dr Merve Mocan for providing the RAFT agent BDAT. Ing. Marco Hendrix is thanked for his help while operating the SAXS equipment at TU/e ICMS, Eindhoven, The Netherlands. Dr Pieter de Waard is thankfully acknowledged for his help with the NMR measurements at the magnetic resonance facility MAGNEFY in Wageningen, The Netherlands. This research was financially supported by the Netherlands

Organization for Scientific Research (NWO) *via* a Vidi innovational research grant.

References

1 E. Spruijt, M. A. C. Stuart and J. van der Gucht, *Macromolecules*, 2013, **46**, 1633–1641.
2 J. van der Gucht, E. Spruijt, M. Lemmers and M. A. C. Stuart, *J. Colloid Interface Sci.*, 2011, **361**, 407–422.
3 E. Spruijt, A. H. Westphal, J. W. Borst, M. A. C. Stuart and J. van der Gucht, *Macromolecules*, 2010, **43**, 6476–6484.
4 R. J. Stewart, C. S. Wang and H. Shao, *Adv. Colloid Interface Sci.*, 2011, **167**, 85–93.
5 S. Kaur, G. M. Weerasekare and R. J. Stewart, *ACS Appl. Mater. Interfaces*, 2011, **3**, 941–944.
6 A. S. Hoffman, *Adv. Drug Delivery Rev.*, 2012, **64**, 18–23.
7 D. Priftis and M. Tirrell, *Soft Matter*, 2012, **8**, 9396–9405.
8 A. H. Hofman, I. A. van Hees, J. Yang and M. Kamperman, *Adv. Mater.*, 2018, **30**, 1704640.
9 I. K. Voets, P. M. Moll, A. Aqil, C. Jerome, C. Detrembleur, P. de Waard, A. de Keizer and M. A. C. Stuart, *J. Phys. Chem. B*, 2008, **112**, 10833–10840.
10 A. Harada and K. Kataoka, *Macromolecules*, 1995, **28**, 5294–5299.
11 D. V. Pergushov, A. H. E. Muller and F. H. Schacher, *Chem. Soc. Rev.*, 2012, **41**, 6888–6901.
12 N. Rapoport, *Prog. Polym. Sci.*, 2007, **32**, 962–990.
13 J. S. Park, Y. Akiyama, Y. Yamasaki and K. Kataoka, *Langmuir*, 2007, **23**, 138–146.
14 S. Bayati, K. E. Bergquist, K. Z. Zhu, B. Nystrom, J. S. Pedersen, L. Galantini and K. Schillen, *J. Polym. Sci., Part B: Polym. Phys.*, 2017, **55**, 1457–1469.
15 G. Masci, S. De Santis and C. Cametti, *J. Phys. Chem. B*, 2011, **115**, 2196–2204.
16 H. Dautzenberg, Y. B. Gao and M. Hahn, *Langmuir*, 2000, **16**, 9070–9081.
17 S. De Santis, R. D. Ladogana, M. Diociaiuti and G. Masci, *Macromolecules*, 2010, **43**, 1992–2001.
18 C. Dahling, G. Lotze, H. Mori, D. V. Pergushov and F. A. Plamper, *J. Phys. Chem. B*, 2017, **121**, 6739–6748.
19 J. Li, W. D. He, N. He, S. C. Han, X. L. Sun, L. Y. Li and B. Y. Zhang, *J. Polym. Sci., Part A: Polym. Chem.*, 2009, **47**, 1450–1462.
20 M. Kamimura, J. O. Kim, A. V. Kabanov, T. K. Bronich and Y. Nagasaki, *J. Controlled Release*, 2012, **160**, 486–494.
21 M. A. Ward and T. K. Georgiou, *Polymers*, 2011, **3**, 1215–1242.
22 K. J. Krzyminski, M. Jasionowski and A. Gutowska, *Polym. Int.*, 2008, **57**, 592–604.
23 T. Patel, G. Ghosh, S. Yusa and P. Bahadur, *J. Dispersion Sci. Technol.*, 2011, **32**, 1111–1118.
24 J. Adelsberger, A. Kulkarni, A. Jain, W. N. Wang, A. M. Bivigou-Koumba, P. Busch, V. Pipich, O. Holderer, T. Hellweg, A. Laschewsky, P. Muller-Buschbaum and C. M. Papadakis, *Macromolecules*, 2010, **43**, 2490–2501.
25 H. Feil, Y. H. Bae, J. Feijen and S. W. Kim, *Macromolecules*, 1993, **26**, 2496–2500.
26 M. Cetintas, J. de Grooth, A. H. Hofman, H. M. van der Kooij, K. Loos, W. M. de Vos and M. Kamperman, *Polym. Chem.*, 2017, **8**, 2235–2243.
27 J. T. Lai, D. Filla and R. Shea, *Macromolecules*, 2002, **35**, 6754–6756.
28 A. D. Filippov, I. A. van Hees, R. Fokkink, I. K. Voets and M. Kamperman, *Macromolecules*, 2018, **51**, 8316–8323.
29 Y. J. Zhang, S. Furyk, D. E. Bergbreiter and P. S. Cremer, *J. Am. Chem. Soc.*, 2005, **127**, 14505–14510.
30 H. G. Schild, *Prog. Polym. Sci.*, 1992, **17**, 163–249.
31 E. Spruijt, *Strength, structure and stability of polyelectrolyte complex coacervates*, Wageningen University, Wageningen, 2012.
32 C. M. Li, N. J. Buurma, I. Haq, C. Turner, S. P. Armes, V. Castelletto, I. W. Hamley and A. L. Lewis, *Langmuir*, 2005, **21**, 11026–11033.
33 H. Wu, J. M. Ting, O. Werba, S. Q. Meng and M. V. Tirrell, *J. Chem. Phys.*, 2018, **149**, 163330.
34 D. V. Krogstad, N. A. Lynd, S. H. Choi, J. M. Spruell, C. J. Hawker, E. J. Kramer and M. V. Tirrell, *Macromolecules*, 2013, **46**, 1512–1518.
35 A. V. Ruzette, S. Tence-Girault, L. Leibler, F. Chauvin, D. Bertin, O. Guerret and P. Gerard, *Macromolecules*, 2006, **39**, 5804–5814.
36 J. K. Kim, H. H. Lee, S. Sakurai, S. Aida, J. Masamoto, S. Nomura, Y. Kitagawa and Y. Suda, *Macromolecules*, 1999, **32**, 6707–6717.
37 F. M. Abuzaina, A. J. Patel, S. Mochrie, S. Narayanan, A. Sandy, B. A. Garetz and N. P. Balsara, *Macromolecules*, 2005, **38**, 7090–7097.

